J. Fluid Mech. (1988), *vol.* 197, *pp.* 81–104
Printed in Great Britain

Modifications to the wake of a wire across Poiseuille flow due to a unipolar space charge

By F. M. J. McCLUSKEY AND P. ATTEN
Laboratoire d'Electrostatique et de Matériaux Diélectriques†, CNRS, 166 X-38042 Grenoble Cedex, France

(Received 16 October 1985 and in revised form 9 May 1988)

A wake behind a wire in a developed Poiseuille flow is examined with and without ionic injection into the liquid by the wire. Mean electric fields of up to 50 kV/cm between the wire and two plate electrodes on either side were used to bring about this injection. The resulting Coulomb force can modify the wake flow in two ways. When this force is weak, the injected ions are transported downstream in a thin charged wake, the only effect being that the deficit velocity is compensated over shorter distances. Once the Coulomb force is strong, there are two charged and turbulent plume-like structures going from the wire to the plates. These are perpendicular to the plates for zero forced flow and are pushed downstream to smaller angles as the forced flow is increased. The wake in this case is not present. Different experimental laws are given to characterize the different regimes and the transition between them.

1. Introduction

Under certain conditions, the application of an electric field between metallic electrodes placed in an insulating liquid causes the injection into this liquid of ions of one sign at an electrode (Denat, Gosse & Gosse 1979; Théoleyre & Tobazéon 1983). Under the influence of the electric field, this 'injected space charge' will move to the opposite electrode, generally entraining an intense movement of the liquid itself, which results in the augmentation of charge transport between the electrodes. These electrohydrodynamic (EHD) phenomena (ion injection accompanied by electroconvection) occur in insulating liquids (in practice, liquids of very low electrical conductivity) with typical current densities of the order of a few μA per cm^2. Magnetic effects in the system are thus negligible.

The driving force behind the movement is the Coulomb force (charge density × electric field). There is practically no production of charge in the liquid bulk, the ion source being a solid–liquid interface and creation of charge being due to electrochemical processes there (injection). There have been some studies on electroconvective motion in the case of space-charge-limited (i.e. very strong) injection, in particular between planar, parallel electrodes, and these show that a marked increase occurs in charge transport due to liquid movement (Lacroix, Atten & Hopfinger 1975; Hopfinger & Gosse 1971). Many papers deal with detailed treatments of the problems of EHD stability and electroconvection in the case of strong, pure unipolar injection for different test-cell electrode configurations, liquids, electric field strengths etc. (Atten & Moreau 1972; Schneider & Watson 1970;

† Laboratory also associated with the Scientific, Technological and Medical University of Grenoble (USTMG).

Watson, Schneider & Till 1970; Atten 1975; Atten & Lacroix 1979; Haïdara & Atten 1985; Atten & Haïdara 1985).

Electroconvective phenomena are to be observed in a large number of industrial processes: ion pumps, heat exchangers, mixers, etc. We are interested here in the interactions between a forced flow and an electroconvective one in the particular geometry of a wire between two plate electrodes. The original motivation for our work was to simulate the injection zone of an electrohydrodynamic generator (McCluskey & Atten 1985). We have already characterized to some degree the flow structures occurring in this case (McCluskey & Atten 1984). Note that the results may also give an insight into what happens to the mean flow in a wire–plate electrostatic precipitator (Atten, McCluskey & Lahjomri 1987).

There are two other previous experimental investigations of such interactive flows. Honda (1976) and Atten & Honda (1982) took measurements of the resulting augmentation in pressure drop due to ion injection by one wall of a rectangular channel in a plane Poiseuille flow and the subsequent movement of this space charge under the influence of the applied electric field. At high enough applied voltages V, the Poiseuille flow destabilizes and the subsequent secondary flow leads to an increase in pressure drop of up to a factor of 20. This study gave the explanation for the so-called electroviscous effect (i.e. increase in apparent viscosity). Two types of cellular movement were visualized: stable longitudinal rolls and, for higher V, mobile transverse striations were superposed on this. A second such study was carried out by Atten & Malraison (1981) who noted that, downstream of the injection zone entry, the longitudinal rolls destabilize and the movement appears to have the form of a network of polygonal cells. Remarkably, the cellular flow was broken up only when the mean velocity of the Poiseuille flow was about three times greater than the maximum velocity that exists in a typical convective cell without cross-flow. This shows the strength of the electrical forces and their tendency to engender three-dimensional convection.

In a previous paper (McCluskey & Atten 1984) different flow structures were evidenced depending on the applied voltage and the cross-flow in a wire between a two-plate electrode geometry. This showed the very active role played in the fluid movement by the space charge. These mainly electrical results will be recalled at the start of each corresponding section in what follows. Before entering into the experimental details (§3) we shall first give an account of the phenomena involved in EHD. Section 4 is concerned with the characterization of the electroconvective flow between a wire and two plates, and §5 with that of the wake downstream of the wire in Poiseuille flow with no-electrical forces acting. Section 6 deals with the interactions between the cross-flow and the electroconvective one when the latter is weak or strong.

2. Some fundamental EHD phenomena

In water and in solvents of high enough conductivity, σ, the application of a low or moderate electric field gives rise to an ohmic response, i.e. the electrical current density is given by $j = \sigma E$. The liquid bulk in this case is electroneutral. This is no longer true when working with dielectric liquids of low conductivity and/or high enough electric fields. The current varies non-linearly with the field E and a space charge (referring to free charge) is present within the liquid. This can be understood simply by comparing the relaxation time of the liquid τ (where $\tau = \epsilon/\sigma$: ϵ is liquid permittivity) with the ionic transit time from one electrode to the other, t_T (where

$t_T = d^2/KV$: d is the electrode gap distance; K the ionic mobility and V the applied voltage). In the first case mentioned above, τ is much smaller than t_T and any space-charge perturbation disappears rapidly. Conversely, when τ is greater than t_T, the space-charge perturbations do not relax and consequently, the space charge occupies the major part of the liquid bulk.

Two mechanisms of ion creation can give rise to the buildup of space charge: (i) the process of dissociation of a neutral species in the liquid bulk with a related recombination of the generated charge carriers, and (ii) the phenomenon of ion injection by the electrodes, a process which is electrochemical in nature. The study of electrical conduction of dielectric liquids between metallic electrodes revealed the universal character of the injection process (Félici 1971*a*) and the general dominance of injection by one electrode only, cathode or anode. Therefore, it is usual to assume as here, for example, that we have unipolar injection (or injection of ions of one sign only) into an insulating liquid. This asymptotic case has been well verified experimentally by using ionically purified liquids into which ions are injected at one electrode. Such injections could be obtained via the photoelectric effect, via radioactive substances etc. We restrict ourselves to an injection process activated by the electric field.

With polar liquids ($\epsilon > 4$), an ion-exchange membrane covering the electrodes provides strong injection (Félici 1971*a*). In non-polar liquids, the addition of some salts (Denat *et al.* 1979) results in a field-controlled injection of low or moderate level by metallic electrodes. Generally, as the injection at a metal–liquid interface is electrochemical, the level of injection greatly increases with the applied electric field (Théoleyre & Tobazéon 1983). For this reason, reproducible injections are more easily obtained from electrodes of high curvature (wire, blade, needle ...).

If, for example, we consider planar geometry, the charge distribution is such that it decreases in density from the injecting electrode to the collecting electrode, while the electric field increases. This situation is potentially unstable (see for example Atten 1975), and above a certain applied voltage liquid motion will begin, i.e. electrical forces must be strong enough so that the movement of the liquid will not be damped out by viscous dissipation (Atten & Moreau 1972). The ratio between electrical and viscous forces gives the stability parameter $T = \epsilon V/K\eta$, where η is the dynamic viscosity. The numerical value of the critical T-value depends on the injection intensity.

There is an obvious analogy with Rayleigh–Bénard convection here but mention must be made of one very important difference. The ions in the EHD case migrate across the liquid layer with an extra velocity component: the ionic drift velocity (mobility × electric field). Thus, the transport is due to liquid motion (convection), ionic drift relative to the liquid itself and diffusion. This last is normally ignored since a simple order-of-magnitude evaluation shows it to be negligible compared with the other two processes. In the Rayleigh–Bénard case heat is transported by diffusional processes only. The importance of the ionic drift velocity KE is demonstrated in the nonlinear stability analysis of a fluid layer between two plane parallel electrodes (Atten & Lacroix 1979). This shows the existence of a finite-amplitude solution for subcritical conditions.

Beyond the critical stability value T_c (proportional to the applied voltage for a given liquid), two regimes of motion exist depending on the value of the Reynolds number Re constructed with the typical velocity of the liquid w' (this is a local velocity value since, as in Rayleigh–Bénard convection, the mean velocity is zero). For $Re \ll 10$ (with Re = liquid velocity × electrode gap/liquid kinematic viscosity ν)

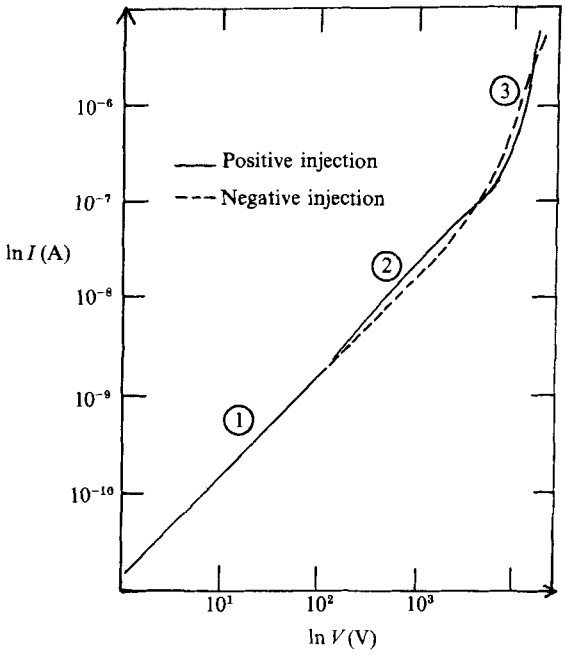

FIGURE 1. Current–voltage characteristics in Benzyle Neocaprate in a blade–plane electrode geometry (after Haïdata & Atten 1985). (1) Ohmic regime; (2) quasi-ohmic regime; (3) injection regime.

the movement is well structured (i.e. cellular) across the liquid layer with a strong correlation between charge and velocity fluctuations ($w' \propto V^2$). The electrical Nusselt number Ne, which is defined similarly to the thermal Nusselt number (ratio of effective current to conduction current without motion), increases proportionally to the square root of the applied voltage (Lacroix *et al.* 1975). When the Reynolds number becomes much greater than 10, the movement is extremely turbulent and the electrical Nusselt number reaches a saturation value ($w' \propto V \propto T \Rightarrow Ne \propto T^0 =$ const, see Lacroix *et al.* 1975).

In non-symmetric geometries, no hydrostatic state is possible and the liquid begins to move once injection occurs. Basic transport processes do not change from the planar case though the structure of the liquid motion depends heavily on the electrode configuration. The study of electroconvective movement in this case is particularly important if one wishes to understand the processes going on, for example, in electrostatic precipitators or EHD high-voltage generators or pumps. Some experiments have already been carried out in a cell comprising a blade in front of a planar electrode (Haïdara & Atten 1985). Figure 1 shows the steady-state variation of current with applied voltage. Three different regimes are evident: an ohmic one, a quasi-ohmic one and a third one where there is dominant injection by the blade and where the current varies according to a power law ($I \propto V^\alpha$, where α can take on values between 3 and 6 depending on the radius of curvature of the blade). The second regime deviates from the ohmic law owing to space charge injected by the blade.

Visualization of the movement showed a liquid plume leaving the blade and inducing two large eddying structures on either side. This (permanent) plume plays a crucial role in the transport of charge and is a major factor in its strong increase.

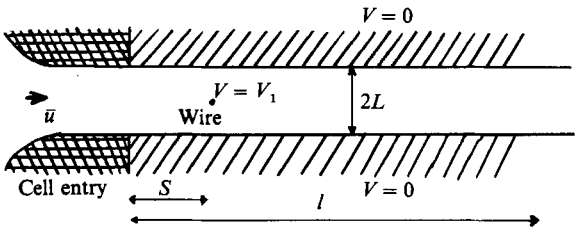

FIGURE 2. Schematic of the cell: wire diameter $\phi = 0.1$ mm; $S = 25$ mm; $2L = 3.5$ mm; $l = 115$ mm.

Velocity measurements within the flow were performed in cases for which the Reynolds number did not exceed 10 for the plume (Atten & Haïdara 1985). Therefore the flow was dominated by viscous effects (though it was probably not laminar in nature). From the form of the Navier–Stokes equation we may deduce the relationship $u \sim qE$. We consider that the current transported, I, is governed by charge convection and we write $I \sim uq$. From these two relations it is simple to derive a relationship between the current and the velocity: $u^2 \propto IV$. This correlation was verified experimentally (Haïdara & Atten 1985) indicating that, to first approximation, the square of the velocity in the plume (proportional to the dissipation of energy by the larger scales in this case) is proportional to the electrical energy furnished. For higher voltages, and thus higher injections and velocities, the flow will become fully turbulent, i.e. $Re > 10$, and we do not expect these laws to hold, though no detailed experiments have been carried out for this inertially dominated regime.

3. Experimental cell and procedures

The cell form and dimensions are given on figure 2. The entry length, i.e. from cell entry to wire, was 8 cm, this being some 23 times the channel width. The entry and exit were profiled to avoid both cavitation and channel entry effects. We verified that the profile just upstream of the wire was a fully developed Poiseuille one for all flow rates in question ($Re < 2000$).

The cell body was made of Teflon with glass windows on each side allowing visualization and optical measurements of the flow. The wire (tungsten, diameter $\phi = 0.1$ mm) was placed between two electrode plates (stainless steel), parallel to them and perpendicular to the oncoming forced flow. The plate electrodes were 3 cm wide (making the wire 3 cm long) and 11.5 cm long. The gap between them was 3.5 mm.

A mechanical pump and flowmeter allowed us to fix the flow rate as desired and the circuit was fitted with a temperature exchanger, allowing us to work at a constant liquid temperature of 22.5 °C. The liquid used, Benzyle Neocaprate (BNC), is a mildly polar one with dynamic viscosity (at 20 °C) $\mu = 6 \times 10^{-3}$ Pa s, mass/unit volume $\rho = 957$ Kg/m^3 and relative permittivity $\epsilon_r = 3.8$. Its resistivity in our operating conditions was about 10^9 Ωm.

We visualized the flow by classical schlieren methods (strioscopy). The wire injector was heated slightly to give the necessary refractive-index difference to the liquid. A d.c. voltage was then applied between the wire and the plates and the movement filmed.

Local measurements of the current density distribution on one of the plate

electrodes were taken as follows: the plane was divided width-wise into a series of small strips parallel to the wire, with each strip being electrically isolated from its nearest neighbours. The current captured by each one was read for given flow velocities and applied voltages.

Measurements of the current entrained out of the cell by the forced flow as a function of voltage were taken. We used a ramp voltage which varied from zero to ten kV continuously and back again over a period of about 10^3 s. This was done for different flow rates. The same quantities were also measured as a continuous function of the flow rate for fixed voltages.

The velocity profiles were determined by laser-Doppler anemometry (LDA). The apparatus used allowed us to measure only the absolute value of the velocity, and we were furthermore limited to working with maximum velocities of the order of 3 m/s (i.e. mean velocities of about 2 m/s). The plate-to-plate distance was too small, given the breadth of the cell, to allow access to the transverse velocity component and only longitudinal velocity profiles are given. For the measurements, we relied mainly on the 'natural' particles in the liquid; no seeding of the flow was necessary. A question, however, arises as to whether the particle velocity accurately represents the true liquid velocity. Particles in an electric field generally become charged and experience a force which causes them to drift with respect to the liquid. In our case, the particles are insulating in nature and their charge is related to their zeta potential (Hunter 1981). With the usual values for this, we obtain drift velocities of the order of 1 mm/s (the particle drift velocity $V_p \approx 3$ mm/s for an electric field of 60 kV/cm). These are always less than 2% of the measured particle velocity (McCluskey 1985) and well within the limits of uncertainty for the measurements of the longitudinal velocity component.

Each velocity value given and the corresponding standard deviation were determined from fifty individual measurements, which required a time of at most three minutes to take. There is a standard deviation for each mean value even for steady-state laminar flow. This is in part due to the instrumentation and in part due to the fact that the zone of measurement (an ellipsoid, $50 \times 50 \times 300$ μm^3) is relatively large, and in regions of high velocity gradient there will be a standard deviation associated with each mean value because of this (this was verified for the case of a Poiseuille flow).

For the various experiments, the Reynolds number of the cross-flow was varied from 0 to about 2000 and the maximum applied voltage was 10 kV. This voltage maximum corresponds to a mean field between wire and plates of approximately 60 kV/cm, the actual field on the wire being substantially higher (Tobazéon 1966). This ensured a strong enough injection by the wire while being comfortably less than the breakdown field strength for this liquid. The current passing through the electrodes comprises a conduction current, due to the fact that the liquid is not a perfect insulator, and an injection one. Up to $V \approx 2$ kV the current is ohmic (or quasi-ohmic) whereafter injection becomes preponderant and the current varies typically as the third or fourth power of V (see figure 1).

4. Unforced electroconvection

4.1. *Visualization*

A 4-roll structure is clearly seen from the photographs of figure 3. The movement was filmed, allowing us to be sure of the direction of the fluid flow. There are two 'charged plumes' going from the wire to the plates, where each separates into two wall jets.

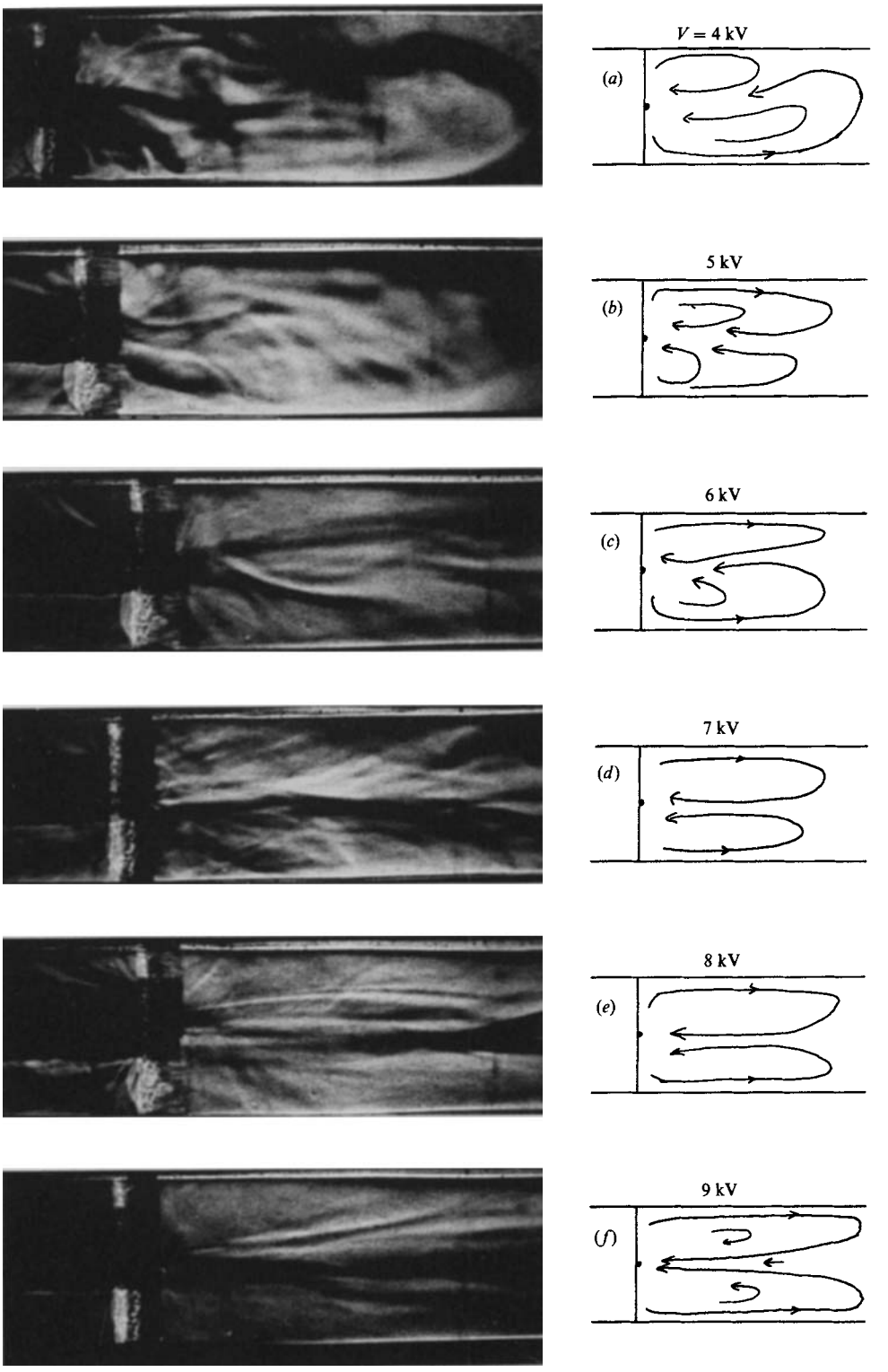

FIGURE 3. Photographs and corresponding streamline sketches of the liquid motion on the right-hand side of the wire for increasing applied voltages.

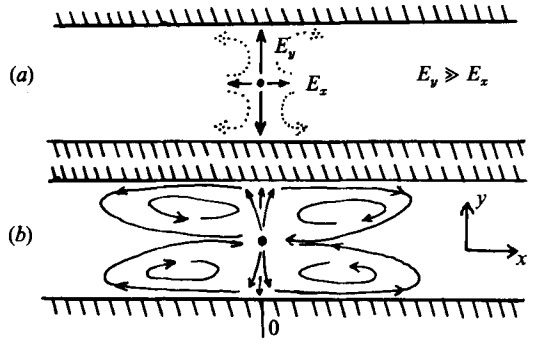

FIGURE 4. (*a*) Sketch of electric field amplitudes in the longitudinal (x) and lateral (y) directions near the wire. (*b*) Schematic of the liquid motion in the form of four rolls.

These latter detach themselves from the plate electrodes eventually and there is a return flow towards the wire along the centre of the canal. This type of movement can be understood as follows. Once voltage is applied between the wire and plates, the resulting electric field is very divergent. If we suppose that the liquid is static, then the field is more intense in the zones between the wire and the plates than along the longitudinal axis of the canal (figure 4). The Coulomb force qE acting on the injected space charge, is also stronger in those zones. The resulting torque causes the liquid to move in this 4-roll structure. The return flow towards the wire in the channel centre will also entrain some of the charges injected in the Ox-direction back into the wire–plate zones, thus augmenting the torque.

From the photographs of figure 3, we see that there is a certain lack of symmetry in the size of the large-scale eddies. This difference is very marked for $V < 5$ kV. It apparently diminishes greatly for $V > 5$ kV. This non-symmetry is not primarily due to a geometrical defect in the cell; repeating the experiment (application of a voltage) a number of times shows that the dominant structure is not always the same. There was however a slight tendency for the upper eddy to be greater than the lower one (over about 25 tests, the upper roll was bigger about 60% of the time). The flow dissymmetry does not apparently affect the currents measured on each plate. These remained constant and equal to each other within the uncertainty of about 1% that exists in the current measurements. We may suppose then, that a symmetric flow organization (i.e. rolls of the same size) does not correspond to a stable state of motion.

From figure 3, we note that the wall jets are visible up to a distance that is a number of times that between the wire and plates (L). This distance increases with the voltage. The movement is turbulent though this is not evident from some of the photographs. Superposed on the large-scale structures, small-scale eddies are visible to the eye for V up to 7 kV. At higher V-values their detection would require the use of a high-speed camera (cf. Hopfinger & Gosse 1971).

The applied voltage for the photographs shown in figure 3 was positive. In the negative case, the movement appeared far more turbulent; no coherent structures were discernable. Though there was no significant difference in the magnitudes of the positive and negative currents, this phenomenon could be caused by non-homogeneous negative injection along the wire surface (A. Denat 1984, private communication).

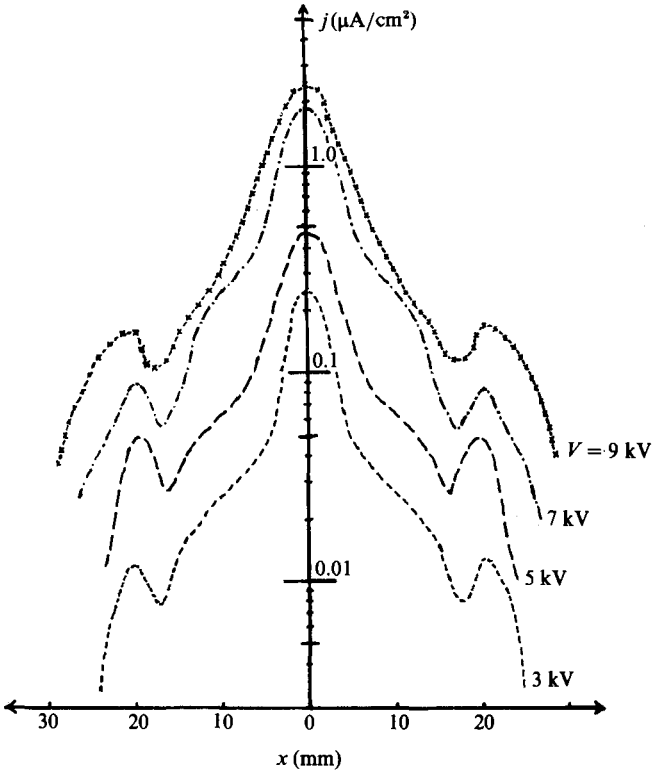

FIGURE 5. Current density distribution along the plate electrodes on either side of the wire for different applied voltages and zero mean flow.

4.2. *Current density measurements*

Shown on figure 5 are the approximate current density distributions for various applied voltages. The curves are symmetric along the plate on either side of the wire. The central maximum in current density corresponds to the zone of impingement of the wire-to-plate 'charged plume'. There is no clear explanation for the presence of the two local maxima downstream, though they could be related to the entrainment of charge within the wall jets.

4.3. *Velocity profiles*

We present on figure 6 a set of approximate longitudinal velocity profiles for an applied negative voltage of 9 kV. The unambiguously determined parts of these profiles are the two wall jets and the central return flow, where the instantaneous longitudinal velocity component does not change in sign. In those zones where it does change in sign, the 'approximate' expected velocity profile is marked with a dotted line. We took a number of profiles for the same value of $x\,(>0)$ at different stations parallel to the wire. There was no particular difference between the profiles, indicating that the non-homogeneous negative injection by the wire did not influence the mean flow, the induced perturbations being confined to the lower lengthscales.

From figure 6, we see that the wall jets each occupy about 25% of the channel width near to the wire and widen slowly with distance downstream. This width θ, defined as the half-width and estimated from a series of 'averaged, symmetrical' curves, varies as x^m, where $m = 0.15 \pm 0.05$ (figure 7). Thus, the 'confined' wall jet

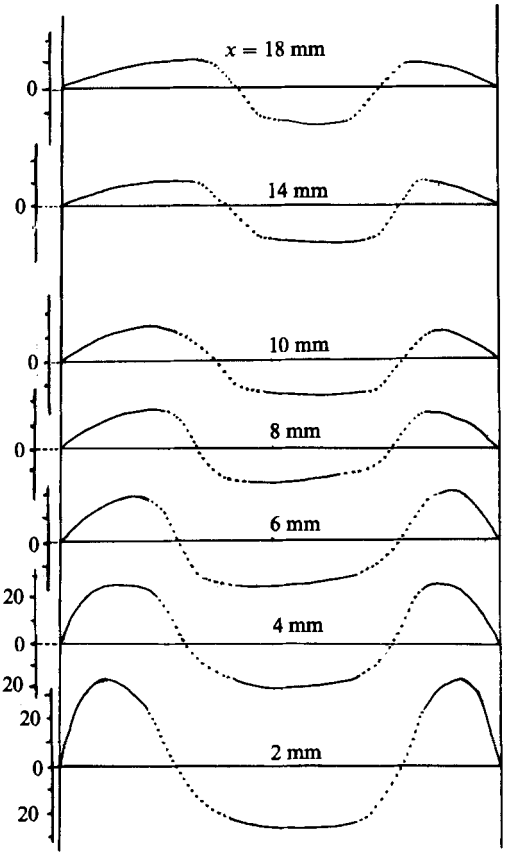

FIGURE 6. Profiles of the longitudinal component of velocity for an applied voltage of 9 kV at different downstream distances. $L = 1.75$ mm.

(return flow in channel centre) enlarges far more slowly than the classical wall jet which has a variation of $x^{\frac{3}{4}}$ in the laminar case (Glauert 1956; Bajura & Szewezyk 1970) and x^1 for turbulent flow (Schwarz & Cosart 1961).

The variation with distance downstream of the maximum velocity in the wall jets obeys a power law x^{-n}, with $n \approx 0.55$ (figure 7). This value of n agrees quite well with that for turbulent plane wall jets observed by Schwarz & Cosart 1961. This latter result suggests that our 'electrohydrodynamic' wall jet is quite similar to the classical one. The difference in the 'spread' of the jet is clearly expected with an 'outer flow' travelling in the opposite direction to the wall jet. This leads to a far less asymmetric profile in our case, but this seems to have only a weak effect on the inner part of the wall jet itself. The space charge has no influence on the structure of the jet since the longitudinal component of the electric field drops with distance downstream in an exponential manner and therefore the Coulomb force is very weak there. This is probably not the case however near the stagnation point ($x = 0$), where the Coulomb force is expected to be strong.

Though we could not measure the lateral component of velocity we can nevertheless estimate an order of magnitude for this quantity. Assuming that the wire–plate plume exactly divides in two around the stagnation point on the plate electrode and that the plume half-width is approximately 0.8 times the wire-to-plate

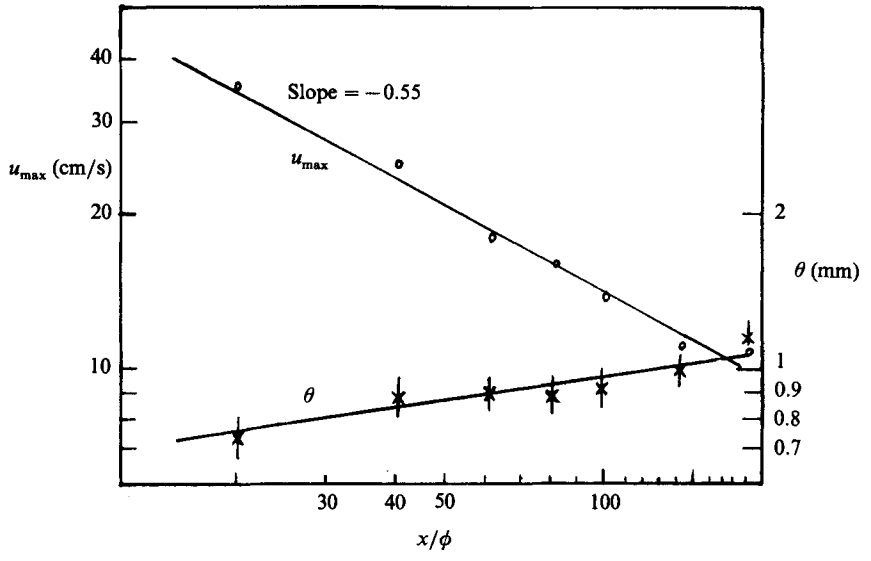

FIGURE 7. Variation with x of the velocity maximum in the wall-jets, u_{max}, and the jet half-width, θ.

distance (Atten & Haïdara 1985), we estimate from mean flow-rate conservation that the maximum velocity in this plume is about 40–50 cm/s for $V = 9$ kV. This value concurs with estimations from previous electrical measurements (McCluskey & Atten 1984).

Since it is rather difficult to evaluate levels of turbulence with a classical LDA measuring system, we prefer not to give any qualitative details on this. We content ourselves with the remark that velocity fluctuations about the mean value were quite significant, indicating that the flow was very turbulent.

5. The wake of a wire across Poiseuille flow

Before examining the interactions between a Poiseuille flow and an EHD plume, it is necessary to look at the wake associated with such a non-uniform velocity profile. This type of flow does not appear to have been the subject of any research previously, so we have no *a priori* reason to assume that this wake will behave as the free plane wake.

5.1. *The confined wake with a uniform incident velocity profile*

Once a cylinder is placed in a channel, the influence of the channel walls may be estimated by looking at the blocking ratio λ, defined as the ratio of the cylinder diameter ϕ to the channel width $2L$. For very low values of λ ($\sim 10^{-2}$) the influence of the walls on the flow development around the cylinder is totally negligible. Most work for higher values of λ is concerned with pressure distributions on the cylinder, the drag coefficients and the stability of the attached eddies behind the cylinder as well as the effects due to its form: circular, square, triangular (Grove *et al.* 1964; Shair *et al.* 1963; Okamoto & Takeushi 1975; Thom 1933; West & Apelt 1982; Richter & Naudascher 1976; Acrivos *et al.* 1968; Davis, Moore & Purtell 1984). In all the papers cited the incident velocity profile on the cylinder was uniform. Very little attention

has been paid to the development of the wake far downstream in the presence of confining walls.

This last point is of particular interest to us since with a blocking ratio of $\lambda = 0.0285$ we expect no modification to the flow in the immediate vicinity of the wire due to the presence of the walls. From the literature cited above we know that this is the case for $\lambda < 0.04$. With respect to the far wake, Camichel, Escande & Ricaud (1925), Thom (1933), Okamoto & Takeushi (1975) did observe that the streamlines of the wake flow began to contract after a certain distance downstream owing to the confining walls; no velocity measurements were given however. Finally, with an aspect ratio of the cylinder (wire) in our case of 300 (ratio of cylinder length to diameter) there will be no influence due to the sidewalls on the central part of the flow (Nishioka & Sato 1974).

5.2. *Velocity profiles behind a wire with an incident Poiseuille flow*

The velocity profiles were determined for several Reynolds numbers of the channel flow (Re from 175 to 740). The corresponding wire Reynolds number (Re_ϕ) therefore varied from about 8 to 32. Since $Re_\phi < 40$, we shall not encounter a Kármán vortex sheet. It has however been shown that a vibration of the wire, under certain conditions, can give rise to vortex shedding for wire Reynolds numbers less than 30 (Dupin & Teissié-Solier 1928; Thom 1933; Taneda 1956). This will occur if the period of the shedding is equal to the harmonic period of vibration of the wire. We estimated the frequency of vibration of our wire to be of the order of 750 Hz, whereas, from the curves given by Dupin & Teissié-Solier 1928, the vortex-shedding frequency would be 2200 Hz at $Re_\phi = 32$. Thus there will be no vibration-induced vortex shedding.

Some typical velocity profiles are given on the left-hand side of the curves in figure 8, at different downstream distances x_i. Before characterizing the confined wake flow development, certain quantities must first be defined. In the free wake the deficit velocity is defined with respect to the outer, undisturbed, uniform velocity. Such a definition is not possible here, so we are left with two other options. We may define the deficit velocity with respect to (i) the maximum velocity measured for each profile or (ii) the Poiseuille flow which would exist without the obstacle. With the second definition, Δu, the deficit velocity, tends to zero as x tends to infinity (cf. the free wake). With the first, Δu increases to zero at some finite value of x. The variation of $\Delta u_{\max}$ is shown on figure 9 for both definitions. In the second case $\Delta u_{\max} \sim x^p$ ($p \approx -0.63$) in the limited range $10 \leqslant x/\phi \leqslant 30$. The first definition appears more satisfactory: $\Delta u_{\max} \sim x^t$ with $t \approx -1$, this law being valid over a clearly greater downstream length, e.g. for $10 \leqslant x/\phi \leqslant 70$ when $Re = 740$.

The second characteristic parameter of a wake is its width δ. We have chosen it to correspond to the velocity value that is halfway between the velocity maxima and minimum. Figure 10 shows that δ varies initially according to a power law x^l ($l \approx 0.25$) before diminishing. This is in accordance with the observations of Dupin & Teissié-Salier 1928, Thom 1933 and Okamoto & Takeushi 1975 for confined 'uniform flow' wakes. Thus, the combined effects of confinement and a parabolic incident velocity profile result in a strong change in the laws governing the development of the wake: $t = -1$ and $l \approx 0.25$ instead of $-\frac{1}{2}$ and $\frac{1}{2}$ respectively.

For $x/\phi < 70$, the wake appears to follow the two laws fairly closely and we may expect that the wake be self-similar in this region. The curve

$$\frac{\Delta u}{\Delta u_{\max}} = \frac{u_{\max} - u}{u_{\max} - u_{\min}}$$

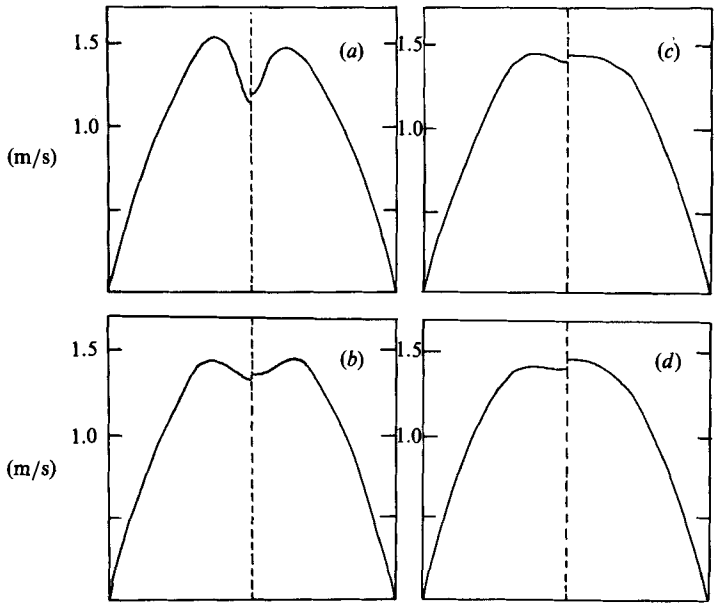

FIGURE 8. Velocity profiles for $Re = 740$ and $V = 0$ kV (left-hand side) and $V = 3$ kV (right-hand side) for different downstream distances. (*a*) $x = 20\phi$; (*b*) 60ϕ; (*c*) 100ϕ; (*d*) 140ϕ. The current captured by each plate was 0.3 μA and the entrained current was 1 μA.

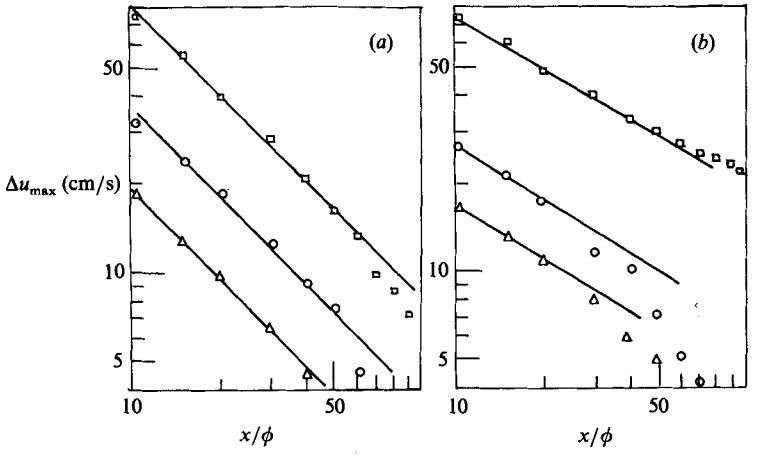

FIGURE 9. Variation of the maximum wake deficit velocity Δu_{max} with x for $Re = 740$ (□), 460 (○) and 175 (△). (*a*) definition (i); (*b*) definition (ii), see text.

as a function of y/δ is shown on figure 11 for different Reynolds-number flows at various downstream distances. All points apparently fall onto the same universal curve and the wake can therefore be reasonably considered as being self-similar.

We noted, finally, that for higher Reynolds-number flows, the wake showed a tendency to veer towards one or other of the confining walls, the profile no longer being symmetric with respect to the channel axis. A similar phenomenon has also been observed in confined jets (Rajaratnam 1976).

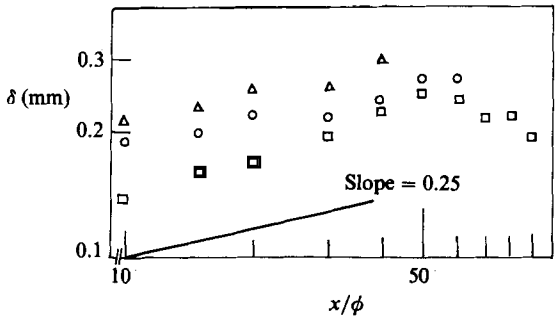

FIGURE 10. Variation of the wake width δ with x for $Re = 740$ (□), 460 (○) and 175 (△).

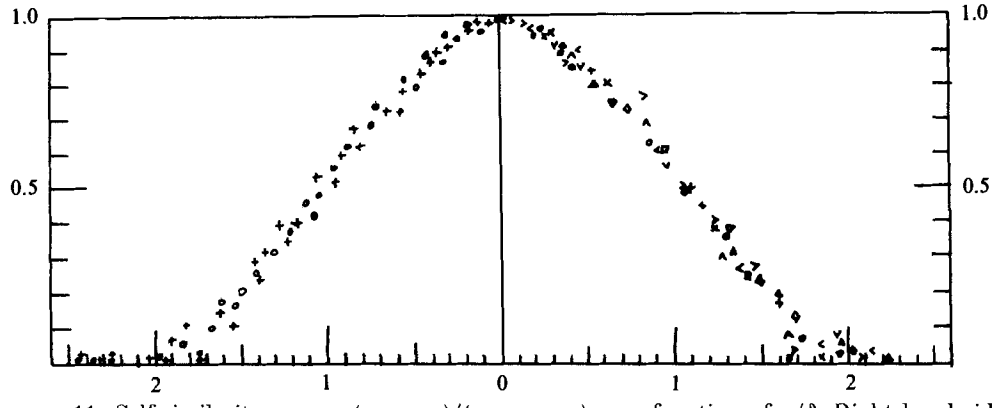

FIGURE 11. Self-similarity curve: $(u_{max}-u)/(u_{max}-u_{min})$ as a function of y/δ. Right-hand side: $Re = 740$, $V = 0$ at: $x = 10\phi$ (<); 15ϕ (>); 20ϕ (□); 30ϕ (◇); 40ϕ (▽); 50ϕ (△); 60ϕ (Λ); 70ϕ (V). Left-hand side: $Re = 740$, $V = 3$ kV (+) at $x = 10\phi$, 20ϕ, 30ϕ, 40ϕ and 50ϕ. $Re = 460$, $V = 0$ kV (○) at $x = 10\phi$, 15ϕ, 20ϕ, 30ϕ, 40ϕ, 50ϕ and 60ϕ.

6. Modification of the cross-flow due to charge injection by the wire

With a voltage applied to the wire, there will be a charge injection into the cross-flow. We would expect the modifications to the wake due to the resulting Coulomb force to depend on the strength of the injection. For example, if we consider the somewhat analogous situation of mixed convection, we may gain some idea of what to expect in the EHD case. Intuitively, a thermal or plume rising from a chimney stack will be inclined depending on the strength of the prevailing cross-winds. In calm conditions, the plume remains almost vertical whereas in a strong wind it is blown almost to the horizontal. More rigorously, work carried out on mixed-convection boundary layers (Kline *et al.* 1967; Arya 1975; Turner 1979 and references therein) shows that there is competition between the cross-flow and the buoyant flow and that thermals will move across the flow according to the comparative strength of each of these.

In our case, with the buoyancy force replaced by the Coulomb force, we might expect to encounter these two extreme cases: weak injection and weak Coulomb force bringing about little modification to the cross-flow, and the opposite case of strong electrical forces completely perturbing it. We shall examine these two cases before considering the nature of the transition (continuous or abrupt) between the two regimes (see also McCluskey & Atten 1984).

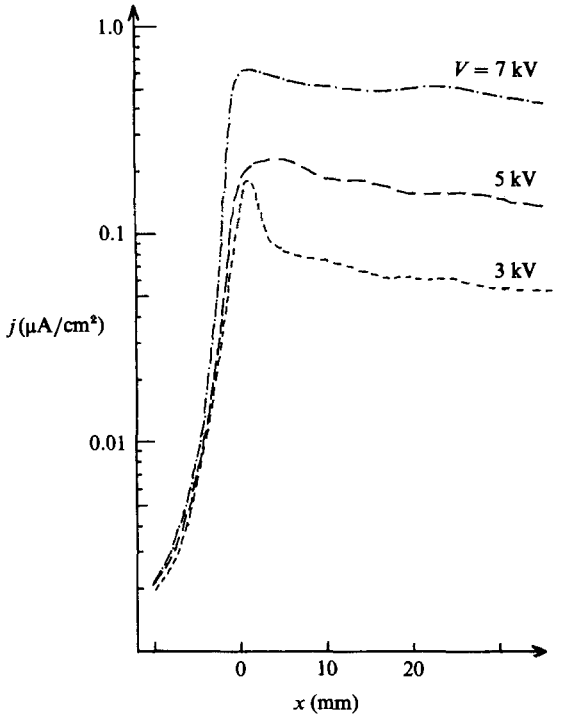

FIGURE 12. Current density distributions along the plate electrode around and downstream of the wire for a cross-flow Reynolds number of 1900 and different applied voltages. The distributions correspond to the entrainment regime and the current ($\propto E$) is due to residual conductivity in the liquid.

6.1. *Weak Coulomb force*

6.1.1. *Current density distribution*

Figure 12 shows some current density measurements with a strong cross-flow (Re = 1900) for three different applied voltages. It takes on a more or less constant value downstream in each case. This would indicate that the injected space charge does not reach the plate electrode, being 'swept' or entrained downstream in a charged sheet in the centre of the channel (figure 13). This will create an electric field between the 'charged sheet' and the plate electrodes that will remain almost constant as long as the charge within the wake does not spread out too quickly. The constant electric field gives rise to a constant conduction current (owing to non-zero residual conductivity of the liquid). This explanation is supported by measurements of the current entrained out of the cell by the forced flow (McCluskey & Atten 1984) and by measurements of the electric field (Tobazéon 1966).

6.1.2. *Velocity measurement*

The wake flow development is essentially the same as in the no-injection case (see right-hand side of profiles in figure 8). There is the difference though, that at any given downstream distance the velocity deficit has a lower amplitude than in the previous case with no electrical forces. This amplitude decreases more as injection is increased. Therefore, wake flows in this regime (effectively represented by low applied voltages) regain a fully developed Poiseuille profile quicker than without injection.

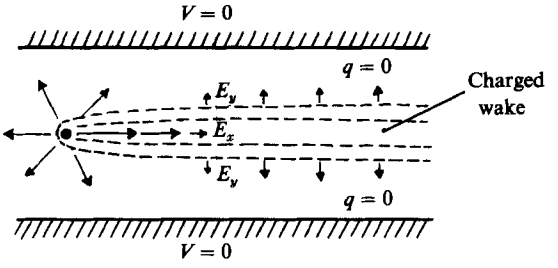

FIGURE 13. Schematic of the electric field E and charge distribution q around and downstream of the wire. (E: full lines; q, broken lines.)

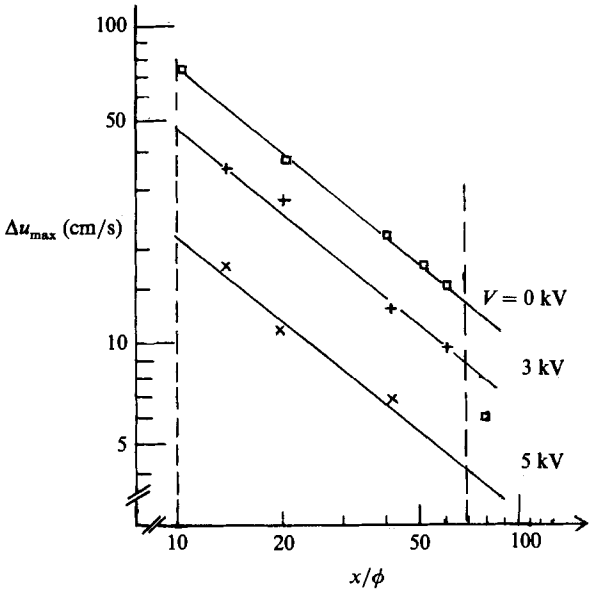

FIGURE 14. Variations of Δu_{max} with downstream distance x for $Re = 740$ and $V = 0$, 3 and 5 kV.

On figure 14 we show the variations of Δu_{max} as a function of x for $V = 0$, 3 and 5 kV at $Re = 740$. Here too, Δu_{max} varies as x^{-1}. The wake width also has the same variation as in the zero-voltage case, i.e. $\delta \sim x^{0.25}$ (results not shown). These laws are valid up to about 50 wire diameters downstream. The values of Δu_{max} (and of δ) diminish with the applied voltage. The profiles are already self-similar at 10 diameters and the non-dimensional curve for the wake is unmodified by the presence of injected space charge (see left-hand side of figure 11). The flow appears to remain laminar since we noted no increase in the fluctuation level around the mean values compared to the no-voltage case, presented in the previous section, except very close to the wire.

We may conclude from these results that the effects of the Coulomb force are limited to a zone of radius of the order of 10 diameters around the wire. In the immediate vicinity of the wire, the field is very intense and radial. Moving away further downstream, the longitudinal component of the electric field E_x decreases rapidly. The injected space charge is entrained downstream behind the wire and passes from a zone where E_x is very high to one where it is negligible, and only the

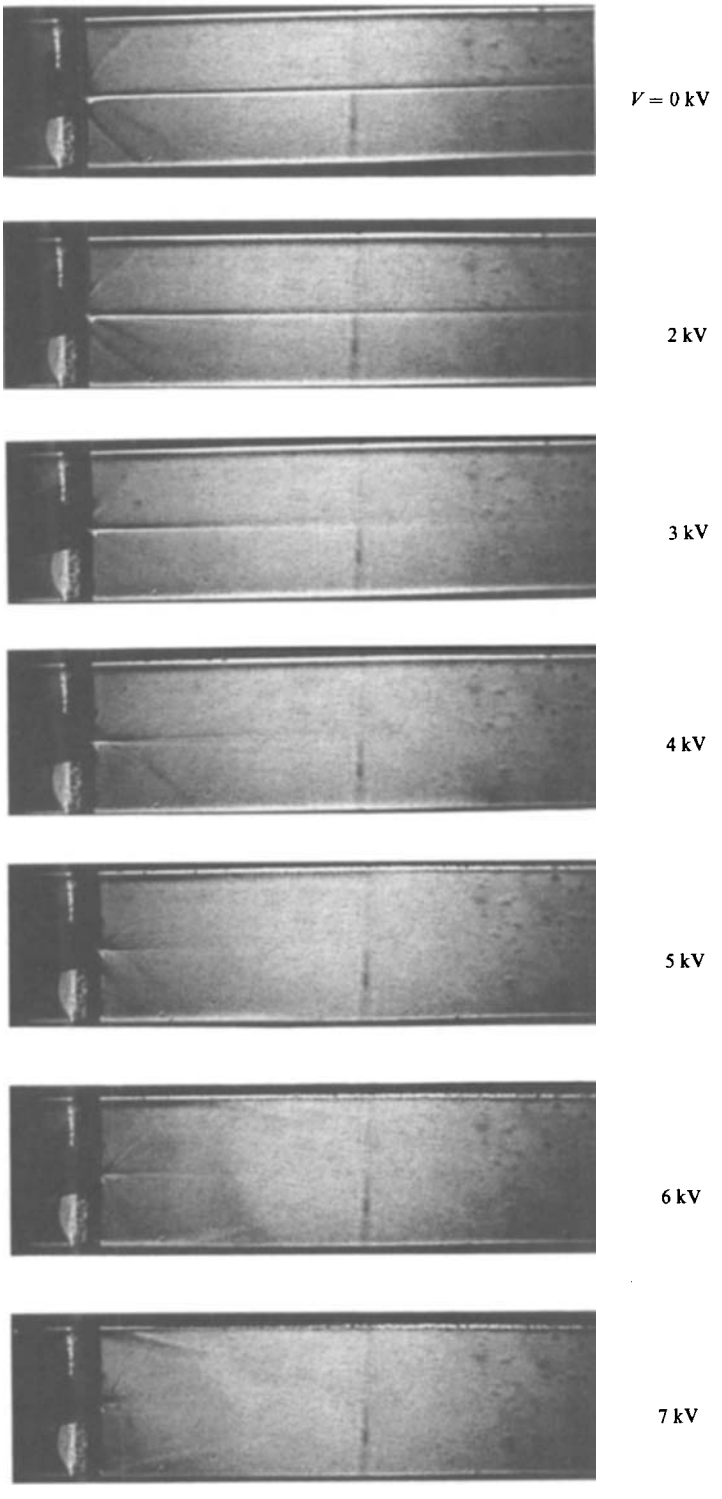

FIGURE 15. Visualization of the wake for $Re = 740$ and different applied voltages. The flow (and wake) is from left to right in the photograph, visible as a sharp white streak along the centre at low voltages.

lateral component E_y exists (figure 13) owing to the presence of the space charge in the channel centre. The component qE_x of the Coulomb force in the vicinity of the wire causes the compensation of the wake deficit velocity there. Of course, the higher V (and hence E_x and q) the greater will be the compensation. Further downstream the effects of the longitudinal Coulomb force are negligible and the space charge is entrained similarly to a passive contaminant. Note that the 'hydrodynamic' and 'charged' wakes do not coincide. The action of the lateral electric field E_y will contribute to the spreading of the charged wake. The 'hydrodynamic' wake increases in width first and then decreases.

6.1.3. *Visualization of the flow*

We attempted to visualize the effects of charge injection on the wake by the Schlieren method (figure 15). For $V = 0$ kV ($Re = 740$), the thermal wake induced by heating the wire spreads very slowly and is visible up to the end of the observation window. With progressively increasing applied voltage, the extension of the wake shortens while its width, presumably, increases. Since the length of the 'visible' wake shortens, then lateral diffusion must have increased; this can only occur near the wire presumably because of small-scale perturbations created there. For $V > 5$ kV, this regime destabilizes and the flow is very turbulent. Observation of the structures with the eye is then impossible even in the area very close to the wire.

6.2. *Strong Coulomb force*

6.2.1. *Current density distribution*

Drastic modifications to the flow occur once the voltage is increased past a 'threshold' value. The current density in this case (figure 16) bears some similarity to the distributions shown in §3 for pure electroconvection. A local maximum reappears downstream while any current injected in the upstream direction is entrained downstream by the forced flow. Since most ($\sim 90\%$) of the injected ions still discharge on the plate electrodes we deduce that the EHD plumes from the wire to the plates are present in some form. We also remark that the abscissa of the first maximum moved downstream with increasing forced flow velocity (for a given applied voltage). This corresponds to the point of impingement of a plume of charge from the wire to the plate being pushed progressively downstream by the forced flow. An order-of-magnitude calculation, where we suppose that the components of the resultant velocity of ions are the mean flow velocity in the downstream direction and a mean transverse velocity v' due to the electrical force, gives the result that $v' = K_{\text{app}} E$ with a value for $K_{\text{app}} \approx 7 \times 10^{-4}$ cm^2/V s, very close to the theoretical EHD value for space-charge-limited injection ($K_{\text{ehd}} = \frac{1}{3}(\epsilon/\rho)^{\frac{1}{2}} = 6 \times 10^{-4}$ cm^2/V s). This rough calculation does not take into account the effects of confinement (i.e. constant flow rate within the canal). A clearer idea of the structure of the movement requires very detailed velocity measurements.

6.2.2. *Velocity measurements*

Typical profiles of the longitudinal component of mean velocity are shown on figure 17 ($V = 9$ kV and $Re = 740$). We have had to average these 'symmetrical' profiles because the flow in this regime is not steady in time (this was not necessary for the profiles shown on figure 8). For example, if we continuously measure the velocity at a given point downstream of the wire, near to the wall, we find that the mean velocity value varies in time (figure 18). The characteristic timescale of the

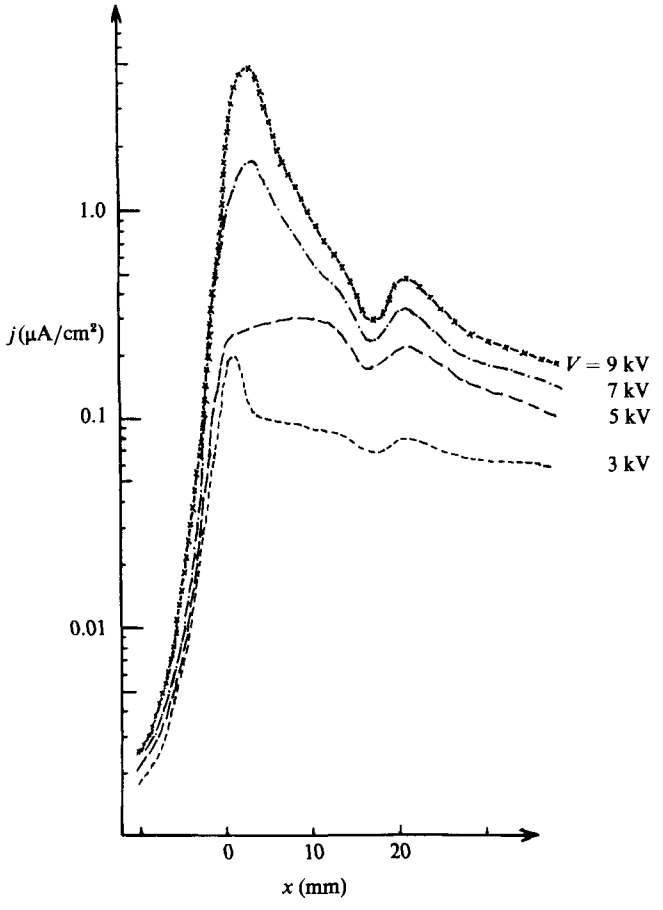

FIGURE 16. Current density distributions along the plate electrode around and downstream of the wire for a cross-flow Reynolds number of 740 and different applied voltages. The distributions correspond to the 'EHD wire-to-plate plume' regime.

variation is a few tens of minutes, a duration greater than that necessary for a single measurement ($\sim$ 1 min). This 'intermittency', which corresponds to very asymmetric instantaneous velocity profiles, does not translate to the current variations on the two-plate electrodes. These currents remain constant and, to within 2%, equal to each other.

The Coulomb force is so intense that the incident Poiseuille flow is totally changed and no wake is evident for $x > L$ (we consider that the relevant scaling length for this regime is L, the wire-to-plate distance, and not the wire diameter ϕ, as in §6.1). Further downstream, the longitudinal velocity component near the walls increases significantly, dropping correspondingly in the channel centre (figure 17). This excess velocity along the plate electrodes would appear to correspond to the presence of wall jets. These jets are absorbed downstream at about 8 or 9 times L, and the mean flow takes on an approximate parabolic aspect at about $x = 12L$.

As in the case of unforced electroconvection (§3), these wall jets are due to the existence of some plume-like structure between the wire and the plate electrodes. If such structures are present, their points of impingement will be moved downstream by the oncoming forced flow. In effect, on the measured profiles the wall jets are not

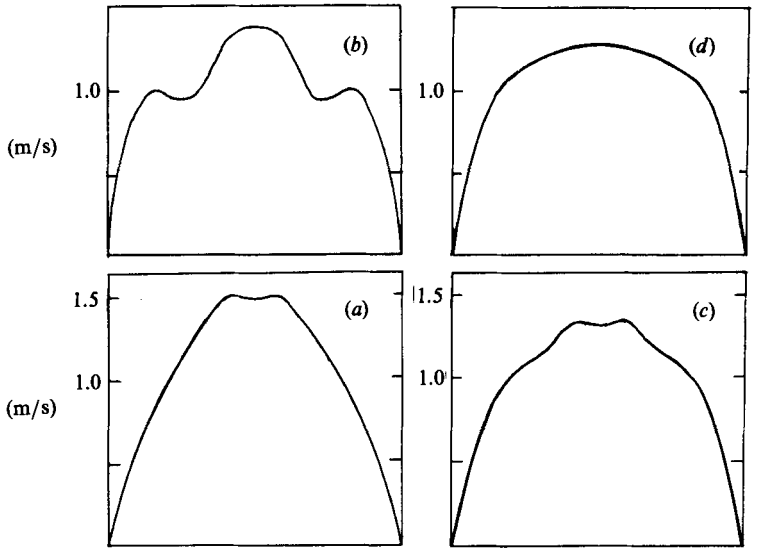

FIGURE 17. Averaged velocity profiles for $Re = 740$ and $V = 9$ kV at (*a*) $x = L$; (*b*) $4L$; (*c*) $6L$; (*d*) $9L$ (where $2L = 3.5$ mm). The current captured by each plate was 8 μA and the entrained current was 0.7 μA.

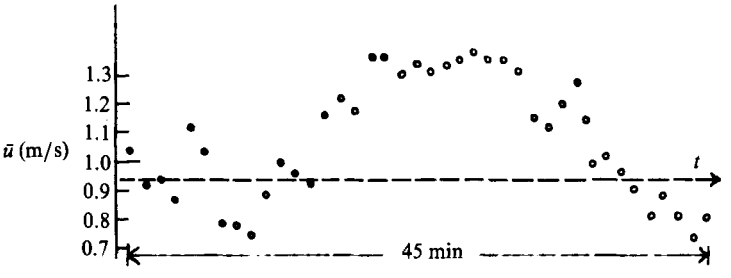

FIGURE 18. Time variation of the instantaneous longitudinal mean velocity component at $x = 7L$ and $y = 0.6$ mm from the wall. $Re = 740$ and $V = 7$ kV. The broken line indicates what the mean value at 0 kV would be at the same point.

evident for $x > 2L$. For $x > 2L$, every profile can be schematically decomposed into a parabolic one and another analogous to the profiles shown on figure 6 (see figure 19). We noted that the maximum velocity in this 'reconstructed' wall jet is of the same order of magnitude as that for unforced electroconvection (~ 50 cm/s). We conclude from these observations that up to $x = 5L$ the mean flow has a non-negligible lateral component. Though this may lead us to supposing the existence of two wire-to-plate plumes, it is far more likely that there are two plumes of charge going from the wire to each plate electrode, which entrain a certain quantity of liquid with them. The direction of these plumes depends on the two electric field components E_x and E_y to which the injected space charge is subject. The streamlines will then diverge around the wire towards the plate electrodes, thus augmenting the longitudinal velocity component along them.

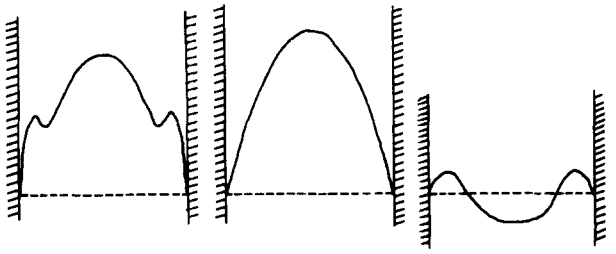

FIGURE 19. Schematic of the decomposition of a typical velocity profile in the first flow regime.

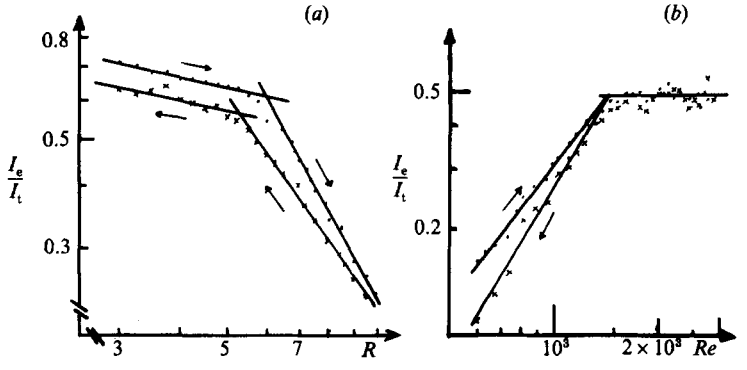

FIGURE 20. Variation of (entrained current/total current) as a function of (*a*) $R(=KV/\nu)$ for a Reynolds number $Re = 2350$, and as a function of (*b*) Re for $R = 5$ corresponding to $V = 5$ kV. (○) Increasing values of R (*a*) and Re (*b*); (×) decreasing values of R (*a*) and Re (*b*).

6.3. *Transition between regimes*

To go from one flow regime to the other the forced flow must be strong enough to break up the plumes of charge going from the wire to the plate electrodes or vice versa. Such a change is probably not very continuous and should be visible from the quantity of total charge entrained out of the cell by the forced flow. Examples of these measurements as a continuous function of R proportional to the applied voltage (R = mobility × voltage/viscosity) and of Re (the Reynolds number of the forced flow) are shown on figure 20. The break in the curves presumably indicates the transition between regimes. From these measurements we found a linear law between Re and R governing the transition (figure 21).

To compare this with similar observations (hexagonal cells and Poiseuille flow, Atten & Malraison 1981) it is necessary to estimate the ratio between the mean cross-flow velocity and the typical wire-to-plate jet velocity in the absence of forced flow. For $V = 9$ kV, this latter velocity was estimated to be about 50 cm/s. For the same voltage, a mean flow of $u \approx 2.5$ m/s was necessary to break up the plumes, leading to a ratio in this case of about five. In their study of the superposition of unipolar injection and a plane Poiseuille flow, Atten & Malraison (1981) estimated that the mean flow had to be about three times greater than the maximum velocity in each hexagonal cell. The higher value in our case may be due to the fact that the secondary structures (wire-to-plate plumes of charge) are two-dimensional. This demonstrates the intensity of the electrical forces and the rigidity of the secondary structures they give rise to.

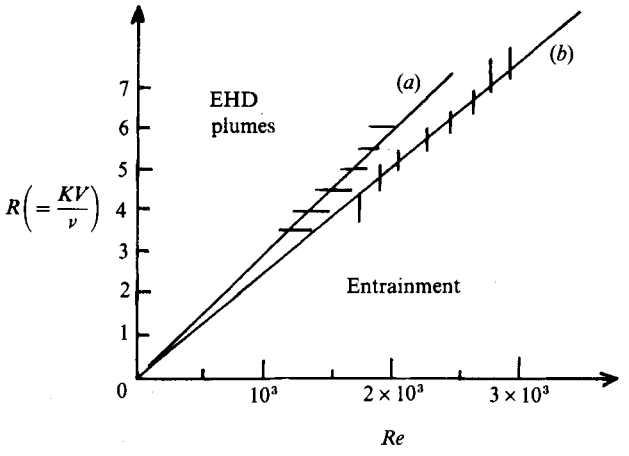

FIGURE 21. Points of transition between the two types of flow regime for (*a*) R fixed and (*b*) Re fixed.

7. Conclusion

We have investigated here the interactions between the electroconvection due to space-charge injection by a wire in a rectangular channel and a laminar cross-flow. It was first necessary to characterize the wake behind the wire for the case of a non-uniform upstream flow before superposing the ion injection. Depending on the applied voltage (or alternatively the resulting Coulomb force), two flow regimes appear. For low voltages, the wake flow is hardly perturbed at all. For high voltages the Poiseuille flow is completely changed: there are two plumes of charge going from the wire to the plate electrodes parallel to it. Intense turbulence is generated in this regime by the very strong Coulomb force. This regime has flow structures and characteristics similar to the unforced electroconvective flow between wire and plates. These 'secondary' structures then resist very strongly the oncoming forced flow.

This work not only has an academic interest in that it examines the interactions between forces not usually encountered in the laboratory but it may also be shown that the results here, using a liquid and ionic charge carriers, are applicable to other types of flow, e.g. a gas with particulate charge carriers. This is particularly important when we consider that complex aerodynamic flows (electrostatic precipitators, electroaerodynamic generators) may be modelled experimentally in the laboratory using properly chosen insulating liquids and test cell geometries.

REFERENCES

ACRIVOS, A., LEAL, L. G., SNOWDEN, D. D. & PAN, F. 1968 Further experiments on steady separated flows past bluff objects. *J. Fluid Mech.* **34**, 25–48.

ARYA, S. P. S. 1975 Buoyancy effects in a horizontal flat plate boundary layer. *J. Fluid Mech.* **68**, 321–343.

ATTEN, P. 1975 Stabilité électrohydrodynamique des liquides de faible conductivité. *J. Méc.* **14**, 461–495.

ATTEN, P. & HAÏDARA, M. 1985 Electrical conduction and EHD motion of dielectric liquids in a knife-plane electrode assembly. *IEEE Trans. Elect. Insul.* **EI-20**, 187–198.

ATTEN, P. & HONDA, T. 1982 The electroviscous effect and its explanation. *J. Electrostatics* **11**, 225–245.

ATTEN, P. & LACROIX, J. C. 1979 Non-linear hydrodynamic stability of liquids subjected to unipolar injection. *J. Méc.* **18**, 469–510.

ATTEN, P., MCCLUSKEY, F. M. J. & LAHJOMRI, A. C. 1987 The electrohydrodynamic origin of turbulence in electrostatic precipitators. *IEEE Trans. Indust. Appl.* **IA-23**, 705–711.

ATTEN, P. & MALRAISON, B. 1981 Superposition d'une injection unipolaire et d'un écoulement de Poiseuille. In *Symmetries and Broken Symmetries in Condensed Matter Physics* (ed. N. Boccara), pp. 503–515. IDSET Paris.

ATTEN, P. & MOREAU, R. 1972 Stabilité électrohydrodynamique des liquides isolants soumis à une injection unipolaire. *J. Méc.* **11**, 471–520.

BAJURA, R. A. & SZEWEZYK, A. A. 1970 Experimental investigation of a laminar two-dimensional plane wall-jet. *Phys. Fluids* **13**, 1653–1664.

CAMICHEL, C., ESCANDE, L. & RICAUD, M. 1925 Sur l'écoulement des fluides visqueux autour d'un obstacle. *C.R. Acad. Sci. Paris* **180**, 1557–1559.

DAVIS, R. W., MOORE, E. F. & PURTELL, L. P. 1984 A numerical–experimental study of confined flow around rectangular cylinders. *Phys. Fluids* **27**, 46–59.

DENAT, A., GOSSE, B. & GOSSE, J. P. 1979 Ion injections in hydrocarbons. *J. Electrostatics* **7**, 205–225.

DUPIN, P. & TEISSIÉ-SOLIER, M. 1928 Les tourbillons alternés de Bénard–Kármán. *Rev. Gén. Electr.* **XXIV**, 53–60.

FÉLICI, N. 1969 Phénomènes hydro- et aérodynamiques dans la conduction des diélectriques fluides. *Rev. Gén. Electr.* **78**, 717–734.

FÉLICI, N. 1971*a* D.C. conduction in dielectric liquids. Part. I. A survey of recent progress. *Direct Curr.* **2**, 90–99.

FÉLICI, N. 1971*b* D.C. conduction in dielectric liquids. Part II. Electrohydrodynamic phenomena. *Direct Curr.* **2**, 147–165.

GLAUERT, M. B. 1956 The wall jet. *J. Fluid Mech.* **1**, 625–643.

GROVE, A. S., SHAIR, F. H., PETERSEN, E. E. & ACRIVOS, A. 1964 An experimental investigation of the steady separated flow past a cylinder. *J. Fluid Mech.* **19**, 60–85.

HAÏDARA, M. & ATTEN, P. 1985 Role of E.H.D. motion in the electrical conduction of liquids in a blade–plane geometry. *IEEE Trans. Indust. Appl.* **IA-21**, 709–714.

HONDA, T. 1976 Etude et interprétation de l'effet électrovisqueux dans les liquides diélectriques isotropes. Ph.D. thesis, Grenoble.

HOPFINGER, E. J. & GOSSE, J. P. 1971 Charge transport by self-generated turbulence in insulating liquids submitted to unipolar injection. *Phys. Fluids* **14**, 1671–1682.

HUNTER, R. J. 1981 *Zeta Potential in Colloid Science: Principles and Applications*, Chap. 3. Academic.

KLINE, S. J., REYNOLDS, W. C., SCHRAUB, F. A. & RUNSTADLER, P. W. 1967 The structure of turbulence boundary layers. *J. Fluid Mech.* **30**, 741–773.

LACROIX, J. C., ATTEN, P. & HOPFINGER, E. J. 1975 Electroconvection in a dielectric liquid layer subjected to unipolar injection. *J. Fluid Mech.* **69**, 539–563.

MCCLUSKEY, F. M. J. 1985 Interaction entre un écoulement forcé et l'électroconvection due à une charge d'espace injectée par un fil entre deux plans parallèles. Ph.D. thesis, Grenoble.

MCCLUSKEY, F. M. J. & ATTEN, P. 1984 Entrainment of an injected unipolar space charge by a forced flow in a rectangular channel. *J. Electrostatics* **15**, 329–342.

MCCLUSKEY, F. M. J. & ATTEN, P. 1985 Velocity profiles in the injection zone of an EHD generator and efficiency considerations. *IEEE Trans. Electr. Insul.* **EI-20**, 405–412.

NISHIOKA, M. & SATO, H. 1974 Measurements of velocity distributions in the wake of a circular cylinder at low Reynolds number. *J. Fluid Mech.* **65**, 97–112.

OKAMOTO, T. & TAKEUSHI, M. 1975 Effect of side walls of wind-tunnel on flow around two-dimensional cylinder and its wake. *Bull. JSME* **18**, 1011–1017.

RAJARATNAM, N. 1976 *Turbulent Jets*. Elsevier.

RICHTER, A. & NAUDASCHER, E. 1976 Fluctuating forces on a rigid circular cylinder in confined flow. *J. Fluid Mech.* **78**, 561–576.

SCHNEIDER, J. M. & WATSON, P. K. 1970 Electrohydrodynamic stability of space charge limited currents in dielectric liquids. 1. Theoretical study. *Phys. Fluids* **13**, 1948–1954.

SCHWARZ, W. H. & COSART, W. P. 1961 The two-dimensional turbulent wall jet. *J. Fluid Mech.* **10**, 481–495.

SHAIR, F. H., GROVE, A. A., PETERSEN, E. E. & ACRIVOS, A. 1963 The effect of confining walls on the stability of the steady wake behind a circular cylinder. *J. Fluid Mech.* **17**, 546–550.

TANEDA, S. 1956 Experimental investigation of the wakes behind cylinders and plates at low Reynolds number. *J. Phys. Soc. Japan* **11**, 302–307.

THÉOLEYRE, S. & TOBAZÉON, R. 1983 Conduction électrique aux champs très intenses dans le carbonate de propylène. *C.R. Acad. Sci. Paris* **296**, II, 241–244.

THOM, A. 1933 The flow past circular cylinders at low speeds. *Proc. R. Soc. Lond.* A **141**, 651–669.

TOBAZÉON, R. 1966 Etude du transfert convectif de charges électriques par un jet de liquide isolant et application à la génération de tensions élevées. Ph.D. thesis, Grenoble.

TURNER, J. S. 1979 *Buoyancy Effects in Liquids.* Cambridge University Press.

WATSON, P. K., SCHNEIDER, J. M. & TILL, H. R. 1970 Electrohydrodynamic stability of space charge limited currents in dielectric liquids. 2. Experimental study. *Phys. Fluids* **13**, 1955–1961.

WEST, G. S. & APELT, C. J. 1982 The effects of tunnel blockage and aspect ratio on the mean flow past a circular cylinder with Reynolds number between 10^4 and 10^5. *J. Fluid Mech.* **114**, 361–377.